Modeling the relationship between substorm dipolarization and dispersionless injection

K. Kabin,[1] E. Spanswick,[2] R. Rankin,[3] E. Donovan,[2] and J. C. Samson[3]

Received 30 May 2010; revised 10 December 2010; accepted 14 January 2011; published 1 April 2011.

[1] Significant populations of electrons with energies of tens of keV appear in the Earth's inner central plasma sheet during the substorm expansion phase. Increasing observational evidence indicates that these injections begin at a radially narrow but azimuthally extended transition between very stretched and less stretched field lines around 8 R_E. In this work we suggest that the tailward retreat of this transition region can be responsible for adiabatic acceleration of electrons which is sufficient to cause ionospheric signatures of the dispersionless injections observed by riometers. To support this mechanism we develop a novel conceptual magnetotail magnetic field model with a few adjustable parameters which can be easily constrained by observations. Our calculations show that a tailward motion of the transition region at the speed of 0.8 R_E/min is required to achieve good agreement with riometer observations.

Citation: Kabin, K., E. Spanswick, R. Rankin, E. Donovan, and J. C. Samson (2011), Modeling the relationship between substorm dipolarization and dispersionless injection, *J. Geophys. Res.*, *116*, A04201, doi:10.1029/2010JA015736.

1. Introduction

[2] In recent years there has been great progress toward understanding the evolution of the substorm [see, e.g., *Angelopoulos et al.*, 2008; *Miyashita et al.*, 2009], however, many of its finer details remain somewhat of a mystery. An important example of this type is the substorm injection, wherein electrons and ions with energies of up to 100 keV appear in the near-Earth magnetotail [*McIlwain*, 1974; *Mauk and Meng*, 1987]. Often, fluxes of particles with different energies increase simultaneously, in which case the injection is called dispersionless. Since gradient-curvature drift speeds of charged particles depend on their energies, dispersionless injections (DIs) would require either local energization of particles or their fast transport.

[3] From the observational point of view, there is increasing evidence about where in the magnetotail DIs occur. While the majority of substorm energetic particle measurements that have been analyzed have been made by geosynchronous (6.6 R_E) satellites [e.g., *Reeves et al.*, 1990], there is no physical reason to associate this distance with the initiation of a DI. A recent survey of satellite data places the typical location of the DI starting point outside the geostationary orbit between 6.6 and 9 R_E [*Spanswick et al.*, 2010]. This result is consistent with other studies, such as an analysis of a smaller sample of satellite data by *Reeves et al.* [1996] and detailed inspections of single events by *Apatenkov et al.* [2007] and *Nakamura et al.* [2009]. The initial location of a DI is believed to be quite narrow in the radial direction; for example using data from radially separated but close satellites [*Reeves et al.*, 1996] estimated the initial radial extent to be no more than 1 R_E.

[4] Further information about DIs has been inferred from ground-based observations of the ionospheric manifestations of the injections. Riometers, for example, are providing some interesting insights into the spatiotemporal evolution of the DI region. Riometers are passive radio instruments which indirectly measure the rate of ionospheric ionization through monitoring ionospheric absorption of VHF (order of 30 MHz) radio waves [e.g., *Alfonsi et al.*, 2008]. Precipitating electrons with energies above 25 keV cause increased ionospheric ionization and, therefore, absorption of the radio waves riometers detect [e.g., *Baker et al.*, 1981]. Thus, DIs of energetic electrons clearly appear in riometer measurements as sudden increases of ionospheric absorption of the radio signal. Riometers have been used to analyze aspects of substorm evolution in the past, for example, by *Hargreaves et al.* [1979] and *Samson and Rostoker* [1983]. More recently, *Spanswick et al.* [2007] showed that DIs in the central plasma sheet (CPS) have an unambiguous riometer signature, such as shown in Figure 1 and described below [see also *Liu et al.*, 2007; *Liang et al.*, 2007]. A typical ionospheric signature of the DI as reported by *Spanswick et al.* [2007], is first detected around 66° geomagnetic latitude and expands poleward ~5° in 5 to 15 minutes; there is also a concurrent, but much smaller (~2° in 5 to 15 minutes), equatorward expansion of the ionospheric signature of the DI. Furthermore, according to *Spanswick et al.* [2007] the riometer signature of DI

[1]Department of Physics, Royal Military College of Canada, Kingston, Ontario, Canada.
[2]Department of Physics and Astronomy, University of Calgary, Calgary, Alberta, Canada.
[3]Department of Physics, University of Alberta, Edmonton, Alberta, Canada.

0148-0227/11/2010JA015736

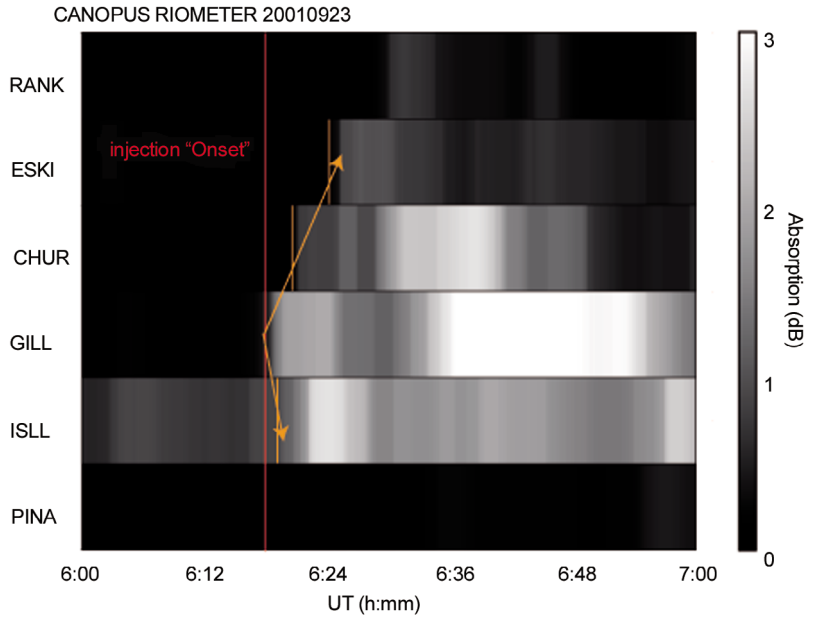

Figure 1. Churchill line riometer measurements during a substorm on 23 September 2001.

initialization has never been simultaneously detected at two different latitudes at the same MLT, thus suggesting that DI starts in a radially thin region of the magnetosphere. The interpretation of this ionospheric signature of a magnetotail process, while subject to caveats related to uncertainties of mapping in a time-evolving magnetic topology, is consistent with that inferred from multisatellite in situ observations [*Reeves et al.*, 1996; *Apatenkov et al.*, 2007; *Spanswick et al.*, 2010]: the DI starts in a radially limited region and expands Earthward (e.g., toward geosynchronous) and tailward. Further support for this scenario is provided by recent observations of the ionospheric total electron content using GPS signals (C. Watson et al., GPS total electron content observation of the evolution of substorm particle injection, submitted to *Journal of Geophysical Research*, 2010).

[5] Optical observations provide a wealth of complimentary information about substorm morphology. The arc that brightens at substorm onset is typically embedded in the poleward "shoulder" of the bright proton aurora that is understood to mark the transition from tail-like to significantly less stretched magnetic field topologies. The onset brightening is usually observed very near to the equatorward boundary of the bright diffuse 630 nm "redline" aurora that is likely the ionospheric footprint of the CPS electrons [see, e.g., *Newell et al.*, 1996; E. Donovan, On the relationship between the central plamsa sheet and diffuse aurora, submitted to *Journal of Geophysical Research*, 2010, and references therein]. There is overwhelming evidence that the ionospheric signature of onset begins on field lines threading the tail-like to less-stretched transition region, dating back to the assertion by *Lui and Burrows* [1978] that the onset began on field lines threading what they referred to as the "nightside cusp." As well the onset arc is typically aligned anomalously close to east–west (compared to arcs observed at other locations or during other geomagnetic conditions) in geomagnetic coordinates [*Donovan et al.*, 2008; *Liang et al.*, 2008], which has been argued to indicate that in the late growth phase, the transition from highly stretched (e.g., thin current sheet region) to less stretched inner CPS magnetic field topologies is restricted to a very narrow radial region (Donovan, submitted manuscript, 2010). Furthermore, there is some in situ evidence that this transition can be very narrow radially [e.g., *Sergeev et al.*, 2003].

[6] Energization of charged particles in DIs is still not entirely understood. While significant modeling efforts in the past were concentrated on acceleration of particles by an earthward propagating electromagnetic pulse [e.g., *Li et al.*, 1998; *Sarris et al.*, 2002; *Zaharia et al.*, 2004], in this paper were explore a different possibility, which is electron energization by a tailward retreat of the inner edge of a thin current sheet. Our paper is organized as follows. We begin by describing our energization scenario in section 2 followed by a presentation of a novel conceptual model (section 3) of the magnetotail magnetic field which incorporates a sharp transition in the radial direction from highly stretched (e.g., thin current sheet) to a less stretched topology. In section 4 we use this model to illustrate the sequence of events during a typical substorm and analyze the feasibility of our DI scenario. The primary focus of section 4 is on explaining the substorm riometer signatures reported by *Spanswick et al.* [2007]. Our findings are summarized in section 6.

2. Local Acceleration of Dispersionless Injection Electrons

[7] The physical mechanism by which the charged particles are energized in DIs is not known. In the last decade, electron and ion acceleration by an earthward propagating electromagnetic pulse has received much attention [e.g., *Li et al.*, 1998; *Sarris et al.*, 2002; *Zaharia et al.*, 2004]. However,

the earthward propagating pulse paradigm appears to be at odds with the recent riometer observations, as its ionospheric signature should be propagating from high to low latitudes. Instead, riometer observations indicate that poleward expansion of DIs is a universal and salient feature of a substorm. Therefore, in this paper we explore an alternative possibility, which is the energization of electrons as a consequence of a tailward retreating inner edge of a thin current sheet. In fact, this view of a dipolarization process has been suggested based on ground-based measurements in early work on substorms by, for example, *Lui* [1978] and is consistent with the riometer and satellite observations summarized in the Introduction. The scenario we envision may or may not be set up by fast earthward convection or local instabilities, but the energization comes from a topological reconfiguration that begins in the inner CPS and occurs at successively greater distances downtail.

[8] It should be noted that the location of the DI initialization is very close to the region where fast earthward flows are decelerated and diverted by the dipole field [e.g., *Shiokawa et al.*, 1997], which is the same location where the transition from stretched to dipole field lines occurs [*Keika et al.*, 2009; *Panov et al.*, 2010]. In fact, the earthward convection probably controls, to some degree, where this transition takes place under various magnetospheric conditions. Magnetospheric convection also affects the magnetic field topology which can certainly be quite complicated. However, in our first attempt at explaining the DIs by local betatron acceleration we do not include those effects and simply consider the location of the dipole to magnetotail transition as an adjustable parameter in the model described in section 3. We then consider a dipolarization during which this thin transition region retreats tailward, increasing the local magnetic field. As a consequence of the increase in the magnetic field, electrons gain energy to conserve their magnetic moment. Recent multisatellite observations reported by *Apatenkov et al.* [2007] indicate that the local magnetic field magnitude and fluxes of energetic electrons increase simultaneously, suggesting that the betatron acceleration mechanism may play a role in the physics of DIs. Even more conclusive evidence of this process was reported by *Asano et al.* [2010].

[9] Betatron acceleration by a locally increasing magnetic field produces highly anisotropic electron distribution functions with $T_\perp > T_\parallel$. Such distributions are unstable with respect to generation of whistler wave modes as originally shown by *Kennel and Petschek* [1966]. These whistler waves are effective in scattering electrons into the loss cone, which remains full until the anisotropy of the distribution is sufficiently reduced. This process has been extensively studied theoretically [e.g., *Summers et al.*, 2009, and references therein] and has substantial observational support [e.g., *Asano et al.*, 2010]. Thus, in our present work we assume that betatron acceleration of electrons is quickly followed by scattering into the loss cone and thus produces ionospheric signatures in riometer data. We emphasize that our scenario for DI corresponds to a local acceleration process, not transport, of electrons.

[10] In section 4 we give estimations for the model parameters required to reproduce a typical time-evolving meridional profile of riometer absorption. In section 4 we also show that the change of the tail magnetic field during a dipolarization is sufficient to accelerate electrons to energies consistent with the riometer signatures of DIs. We note that the magnetotail model described in this section is used only as an illustration and a feasibility demonstration for the proposed DI electron energization scenario. A detailed calculation of electron energization requires introduction of many additional poorly known parameters (such as details of the seed population) and is left for a future study.

3. Magnetotail Model Description

[11] In this section we describe a new simple model of the magnetotail magnetic field. Although there are multiple models of the magnetospheric magnetic field, such as observation-constrained Tsyganenko models [e.g., *Tsyganenko and Stern*, 1996] or global circulation models based on the first principles [e.g., *Toth et al.*, 2005], they are not very well suited for the present study as they allow only indirect control, usually through the solar wind conditions, of such parameters as magnetotail thickness and location. For testing the conceptual mechanism responsible for substorm DIs we need a simple model of the magnetotail with direct and explicit control of magnetotail thickness and, most importantly, the location of the transition from dipole-like to tail-like fields, which is hard, if not impossible, to achieve in the more realistic Tsyganenko and global circulations models. In some aspects, our magnetotail model has similarity to the models used by *Luhmann and Friesen* [1979] and *Wanliss et al.* [2000], although the method of computing the magnetic field is completely new.

[12] For simplicity, we write the equations in the midnight meridian plane and assume axial symmetry in the vicinity of this meridian. As a first step in developing our magnetotail model we define an auxiliary field, **b**, consisting of dipole and tail fields.

$$\mathbf{b} = \mathbf{B}_{dip} + \mathbf{e}_x f(x) B_0 \tanh(z/L_z) \tag{1}$$

where x and z are the Cartesian GSM coordinates measured in the Earth radii, $\mathbf{e}_x$ and $\mathbf{e}_z$ unit vectors in the x and z directions, L_z is the thickness of the magnetotail, and B_0 determines the strength of the cross-tail current, $\mathbf{B}_{dip}$ is the dipole field given in the usual spherical coordinates r and θ (colatitude) by

$$\mathbf{B}_{dip} = B_D \frac{3\sin\theta\cos\theta}{r^3}\mathbf{e}_x + B_D \frac{3\cos^2\theta - 1}{r^3}\mathbf{e}_z$$

B_D = 31000 nT and $f(x)$ is a function used to control the location and sharpness of the transition for dipole-like to tail-like fields. A simple choice used in this paper is

$$f(x) = \frac{1}{2}\left(1 - \tanh\frac{x + R_t}{\delta}\right)$$

where R_t is the location of the transition from dipole to tail-like fields and δ is the radial width of this transition. This function asymptotically approaches 0 for $x \gg R_t$ (near Earth region and the dayside) and 1 for $x \ll R_t$ in the tail region (large negative x corresponds to the far tail region).

[13] It should be noted that $\nabla \cdot \mathbf{b} \neq 0$, so **b** is not the magnetic field, but only an auxiliary vector field used as an intermediate step in the calculations. We use it to define the

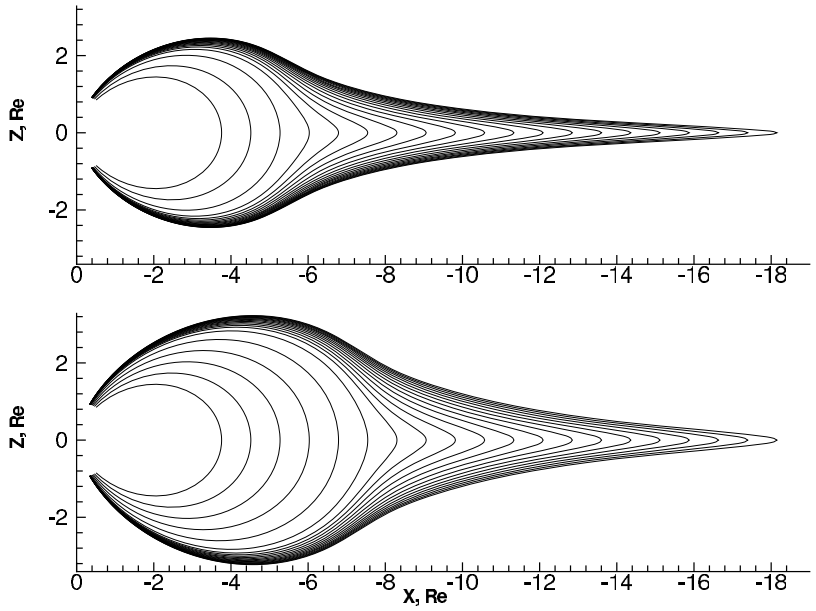

Figure 2. Field lines in the midnight plane (top) before and (bottom) after dipolarization. The parameters for the magnetic field model before the dipolarization were $L_z = 0.25R_E$, $B_0 = -240$ nT, $R_t = 6R_E$, and $\delta = 1R_E$; after the dipolarization, B_0 and R_t were changed to -100 nT and 8 R_E, respectively.

field lines, and as a next step we compute a zero-divergence magnetic field with the same field lines as those of **b**. Specifically, we seek a magnetic field represented in term of Euler potentials, ψ and ϕ, as $\mathbf{B} = \nabla\psi \times \nabla\phi$ [*Stern*, 1970] which is solenoidal by construction. In the axisymmetric case it is convenient to choose ϕ as the azimuthal angle; the corresponding ψ is usually referred to as the flux function. The assumption of azimuthal symmetry is certainly an approximation for the real magnetotail, but for the purposes of our study, which is focused on the midnight region, it can be justified by a large azimuthal extent of the dispersion initiation region and its good alignment with geomagnetic longitude [*Donovan et al.*, 2008; *Liang et al.*, 2008]. In the dipole region, at the surface of the Earth, we can choose $\psi = \sin^2\theta$, the usual expression for a dipole field (for $r = 1$). By definition, the flux function is constant along the field lines, so using the auxiliary field **b** to trace the field lines we can compute the flux function everywhere. The resulting magnetic field, is given by

$$\mathbf{B} = \frac{\nabla\psi \times \mathbf{e}_\phi}{r\sin\theta} = \mathbf{e}_r \frac{\partial\psi}{\partial\theta}\frac{1}{r^2\sin\theta} - \mathbf{e}_\theta \frac{\partial\psi}{\partial r}\frac{1}{r\sin\theta}.$$

This field is by construction solenoidal, and has the same field lines as the auxiliary field **b**. Thus, **B** is parallel to **b** everywhere, but clearly $B \neq b$. The gradient $\nabla\psi$ has to be computed numerically, because we do not have explicit expression for the field lines for the vector field **b**. The above procedure of computing the magnetic field can be applied whenever one wishes to reconstruct a divergence-free field from its field lines.

[14] Although we do not use this property in the present study, the axisymmetric magnetic field model described above corresponds to a plasma equilibrium solution of the Grad-Shafranov equation. Appendix A describes the procedure for computing the corresponding plasma pressure which can be used, for example, for analysis of the stability of the equilibrium. Finally we compute the current density for this magnetic field as

$$\mu_0\mathbf{J} = \nabla\times\mathbf{B} = -\mathbf{e}_\phi\left(\frac{1}{r\sin\theta}\frac{\partial^2\psi}{\partial r^2} + \frac{1}{r^3}\frac{\partial}{\partial\theta}\left(\frac{\partial\psi}{\partial\theta}\frac{1}{\sin\theta}\right)\right)$$
$$= -\mathbf{e}_\phi r\sin\theta\left(\nabla\cdot\left(\frac{\nabla\psi}{r^2\sin^2\theta}\right)\right)$$

Note that the expression for current is obviously related to the pressure gradient, $\partial p/\partial\psi$, through equation (A1).

[15] Figure 2 shows the field lines in the midnight meridional plane before (Figure 2, top) and after (Figure 2, bottom) the dipolarization. The inner edge of the current sheet was moved in this example from its initial value $R_t = 6\ R_E$ to the final value $R_t = 8\ R_E$; at the same time B_0 changed from -240 to -100 nT (the latter change is consistent with $B_0 \sim R_t^{-3}$ scaling, the same as the scaling of the dipole field with distance). The other parameters of the model were $L_z = 0.25\ R_E$ and $\delta = 1\ R_E$. Note that the field lines shown begin in both plots at the same equatorial locations and, therefore, correspond to different ionospheric latitudes. For the same set of parameters, Figure 3 (top) shows the equatorial strength of the magnetic field before and after the dipolarization compared with the dipole field. The ionospheric latitudes corresponding to the equatorial distances are shown in Figure 3 (middle). Figure 3 (bottom) shows the value of the cross-tail current in the model before and after the dipolarization (positive current is in the dawn to dusk direction). Figures 2 and 3 illustrate that the model described in this section combines considerable flexibility

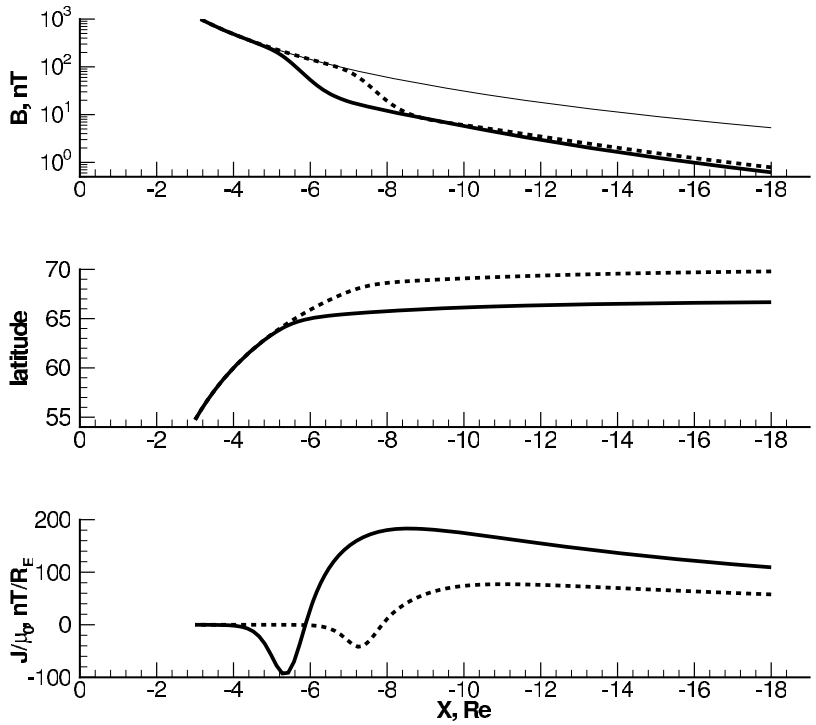

Figure 3. (top) The equatorial magnetic field strength: before the dipolarization (bold solid line), after the dipolarization (bold dashed line), and the dipole field (thin solid line). (middle) Mappings of the equatorial magnetospheric distances to the ionospheric latitudes by the magnetic field model before (solid line) and after (dashed line) the dipolarization. (bottom) Equatorial cross-tail current in the model before (solid line) and after (dashed line) the dipolarization.

with simplicity and easy control of magnetotail parameters, which is essential for our study.

4. Constraining the Model With Observations

[16] In this section we use the model described above to explain some salient features of riometer observations of DIs. Figure 1 shows measurements of riometers along the Churchill line on 23 September 2001. This date was chosen as a particularly clear example of a DI. A survey of 6 years of riometer data by *Spanswick et al.* [2007] shows that the morphology of this event is very typical.

[17] The injection starts around Gillam station at 66° Corrected Geomagnetic latitude and expands by approximately 5° poleward in 6 minutes (the time resolution of the riometer data used is 5 seconds). During the same time interval there is also a much smaller equatorward expansion which we are not considering. The primary focus of our present work is modeling the poleward expansion of the DI in the riometer observations, which is unexpected in the Earthward propagating pulse paradigm.

[18] The physical scenario we consider in this paper for creating DIs of electrons is local betatron acceleration. We assume that throughout the CPS there is an initial population of 10 keV electrons which acts as a seed for the DI. If the local magnetic field increases by a factor of 3, the energy of these seed electrons would reach 30 keV. Electrons with such energies will cause visible signatures of DIs in ground-based riometer observations. The local increase in the magnetic field strength in our scenario is produced by the tailward retreat of the earthward boundary of the cross-tail current sheet. As the earthward current sheet boundary moves tailward across a certain point in space, the local magnetic field at this point changes from tail-like to dipole-like and, therefore, increases. We refer to the ratio of the new to the old magnetic fields as the adiabatic energization factor; for electrons conserving their magnetic moment this ratio also describes their energy increase. For comparison with riometer observations, we track the position of the contour corresponding to the threshold adiabatic energization factor of 3. Our magnetic field model allows easy mapping of the CPS locations to the ionosphere, where the tailward movement of the transition region appears as poleward movement of the threshold adiabatic energization factor, in qualitative agreement with the riometer observations. Finally, we adjust the speed of the tailward motion of the transition region to achieve quantitative agreement with the riometer observations of poleward expansion of the DIs.

[19] Figure 4 shows the adiabatic energization factor obtained in our model by moving the inner edge of the current sheet from 6 to 11 R_E over 6 minutes. The data shown are mapped to the geomagnetic latitude for comparison with the riometer measurements; the latitudes of the riometer stations along the Churchill line are also labeled. The red line corresponds to the threshold energization factor of 3. Note that time dependence appears in our model entirely through the changes in the model parameters and the time shown as the horizontal axis of Figure 4 has been scaled to fit the

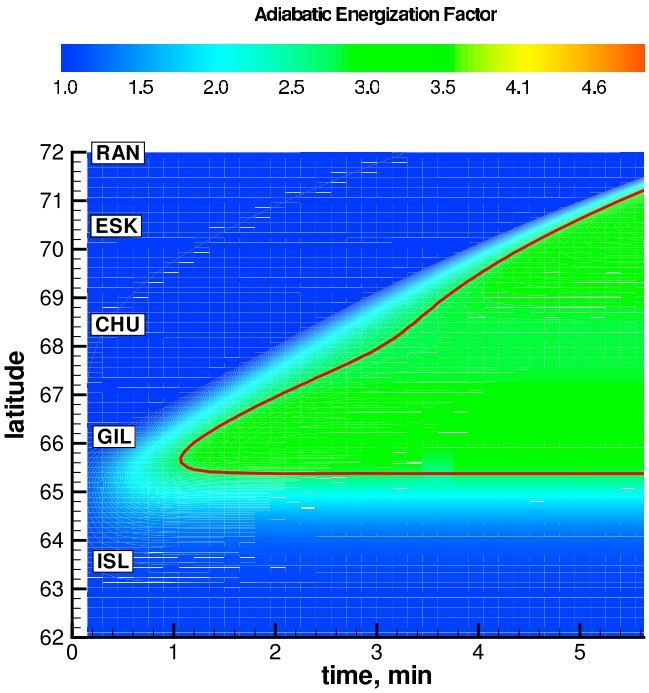

Figure 4. Adiabatic energization factor in the model projected into the ionosphere for comparison with Figure 1. The earthward edge of the current sheet is moved at a constant speed from 6 to 11 R_E.

observations on 23 September 2001. In this particular case, the tailward movement at ~ 0.8 R_E/min is needed to achieve a good comparison with the observations. We note that this is somewhat higher than an average tailward speed of substorm onset reported as 0.3–0.4 R_E/min by *Baumjohann et al.* [1999, 2000] based on a statistical analysis of the Geotail data. It should be noted, however, that this value is an average of a statistical study and individual events can be characterized by significantly different speeds. As reported by *Spanswick et al.* [2007], the expansion phase as seen by riometers varies from about 5 to 15 minutes; and longer times will result in slower expansion speeds. Finally, although *Baumjohann et al.* [1999, 2000] used the best satellite data available at the time, the large distances (both radial and azimuthal) between the individual probes unavoidably introduce significant uncertainties in their estimations.

5. Discussion

[20] The calculation described above demonstrates that change of the local magnetic field as a result of dipolarization can sufficiently increase the energy of CPS electrons to explain riometer observations. Thus, DIs of electrons can be explained by local betatron acceleration alone, without any additional particle transport.

[21] We emphasize that our discussion of DIs is completely independent of the substorm onset mechanism which is outside the scope of the present work. Instead we focus on the morphology of the tail reconfiguration and large-scale particle signatures associated with it. We propose a sequence of events for explaining certain aspects of DIs and use a simple magnetotail model as a proof of concept to demonstrate the physical viability of this scenario. Naturally, there are multiple future extensions of this work. For example, we only considered the adiabatic energization factor at the equator (where it is maximal), while the tailward retreat of the dipole to tail transition region causes the magnetic field to increase at other latitudes as well. The corresponding calculation is straightforward, but adds nothing to the conceptual picture of DIs we describe in this paper. It is, therefore, omitted. Additional electron acceleration may be provided by parallel electric fields, especially in the auroral regions, but such effects are very hard to quantify and are entirely independent of the substorm onset. Another aspect of our discussion above is that the presented process does not produce the earthward expansion of the DI, which is in general significantly more limited spatially than the tailward expansion based on the riometer and satellite measurements [*Spanswick et al.*, 2007, 2009, 2010]. While our scenario produces the bulk of the DI energization, the earthward expansion might be a consequence of a more complicated inner edge topology, or of $\mathbf{E} \times \mathbf{B}$ drift as suggested, for example, by *Reeves et al.* [1996].

6. Conclusions

[22] In this paper we reviewed the phenomenology of electron DIs inferred from satellite as well as ground-based optical and riometer measurements. The observations indicate that DIs start at a radially sharp but azimuthally extended transition region between highly stretched and less stretched field lines. We argue that the radial evolution of the injection region inferred from the ground and in situ observations can be accounted for by a tail reconfiguration (dipolarization) that involves a tailward retreat of the boundary between stretched and less-stretched field lines. Thus, no large-scale particle transport is necessary to account for the observed radial evolution of electron DI.

[23] The late growth and expansion phase of the substorm unfolds in the coupled magnetosphere-ionosphere system on a number of time scales that characterize different physical processes. These time scales range from tens of seconds, for the transition to instability, through minutes and tens of minutes for longer time scale processes such as the dipolarization and evolution of the auroral bulge. The spatiotemporal evolution of the injection that we are modeling is a longer time scale process (~5–15 minutes) which, in our scenario, is inherently coupled to the dipolarizaton. Undoubtedly, there are also shorter time scale processes that operate locally during the dipolarization, but we make no effort here to explore that.

[24] We note that our DI explanation is independent of the substorm onset mechanism, so while we cannot discount the role of transport in the onset of the substorm, we find that it is not required to adequately describe the macroscale radial evolution of the DI region. It is furthermore possible that the variations in size, energy and location of the injection region between individual substorms are a consequence of the characteristics of the magnetic field, such as the radial extent and location of the transition region, and the plasma sheet seed population prior to dipolarization.

[25] To support our view of substorm DIs we developed and implemented a new parametric magnetotail model

which incorporates a radially narrow transition region between highly stretched and nearly dipolar magnetic field lines. Using this model we track effects of a dipolarization, as the dipole field region extends further into the tail. The electron energies in this process increase and we find that this process reproduces the observationally established, key qualitative features of the ionospheric footprint of the DIs with the exception of the relatively small equatorward expansion. We find that tailward motion of the dipole-to-tail transition region with a typical speed of ~0.8 R_E/min is required to achieve agreement with riometer observations. Finally, we emphasize that our electron DI scenario does not require radial transport, nor does it preclude that transport playing a role in setting up the topology. Consequently, our scenario is agnostic in terms of the major substorm models.

Appendix A: Pressure Equilibrium

[26] The magnetic field model described in section 3 is consistent with a plasma equilibrium given by $(\nabla \times \mathbf{B}) \times \mathbf{B} = \nabla P$. In the axisymmetric case this equation can be rewritten as the Grad-Shafranov equation

$$\nabla \cdot \left(\frac{\nabla \psi}{r^2 \sin^2 \theta} \right) = -\mu_0 \frac{\partial p}{\partial \psi}. \tag{A1}$$

[27] The unusual feature of the Grad-Shafranov equation is that the flux function ψ appears in it both as the unknown function and the independent variable. Thus, the most common approach for solving (A1) starts with assuming a particular dependence of the plasma pressure on the flux function, and then solving the resulting (usually nonlinear) Grad-Shafranov equation [e.g., *Krasheninnikov et al.*, 1999]. In our particular case, however, we already know the flux function, so we can apply a reverse procedure. We can directly evaluate the left-hand side of equation (A1) and then use straightforward integration to compute the plasma pressure p (up to an additive constant). In fact, if there were an explicit equation for the field lines of the auxiliary fields (and therefore for the flux function), the problem of computing the pressure would have been reduced to quadratures. Although not used in the current study, the ability to calculate pressure in our model is an important advantage as it is essential for assessing the stability of the magnetotail equilibria as well as including warm plasma effects on the frequency of the field line resonances [*Samson and Dobias*, 2005; *Zhu et al.*, 2009].

[28] **Acknowledgments.** This work was supported by funding from the Canadian Space Agency, NSERC, and the Royal Military College of Canada. We also thank Maj. J. de Boer for his interest in this work and many fruitful discussions.

[29] Masaki Fujimoto thanks Alessandro Retinó and another reviewer for their assistance in evaluating this paper.

References

Alfonsi, L., et al. (2008), Probing the high latitude ionosphere from ground-based observations: The state of current knowledge and capabilities during IPY (2007–2009), *J. Atmos. Sol. Terr. Phys.*, *70*, 2293–2308.

Angelopoulos, V., et al. (2008), Tail reconnection triggering substorm onset, *Science*, *321*, 931–935.

Apatenkov, S. V., et al. (2007), Multi-spacecraft observation of plasma dipolarization/injection in the inner magnetosphere, *Ann. Geophys.*, *25*, 801–814.

Asano, Y., et al. (2010), Electron acceleration signatures in the magnetotail associated with substorms, *J. Geophys. Res.*, *115*, A05215, doi:10.1029/2009JA014587.

Baker, D. N., P. Stauning, E. W. Hones, P. R. Higbie, and R. D. Belian (1981), Near-equatorial, high-resolution measurements of electron precipitation at L ≃ 6.6, *J. Geophys. Res.*, *86*, 2295–2313.

Baumjohann, W., M. Hesse, S. Kokubun, T. Mukai, T. Nagai, and A. A. Petrukovich (1999), Substorm dipolarization and recovery, *J. Geophys. Res.*, *104*, 24,995–25,000.

Baumjohann, W., T. Nagai, A. A. Petrukovich, T. Mukai, T. Yamamoto, and S. Kokubun (2000), Substorm signatures between 10 and 30 Earth radii, *Adv. Space Res.*, *25*, 1663–1666.

Donovan, E., et al. (2008), Simultaneous THEMIS in situ and auroral observations of a small substorm, *Geophys. Res. Lett.*, *35*, L17S18, doi:10.1029/2008GL033794.

Hargreaves, J. K., H. J. A. Chivers, and E. Nielsen (1979), Properties of spike events in auroral ratio absorption, *J. Geophys. Res.*, *84*, 4245–4250.

Keika, K., et al. (2009), Observations of plasma vortices in the vicinity of flow-braking: A case study, *Ann. Geophys.*, *27*, 3009–3017.

Kennel, C. F., and H. E. Petschek (1966), Limit on stably trapped particle fluxes, *J. Geophys. Res.*, *71*, 1–28.

Krasheninnikov, S. I., P. Catto, and R. D. Hazeltine (1999), Plasma equilibria in dipolar magnetic configurations, *Phys. Rev. Lett.*, *82*, 2689–2692.

Li, X., D. N. Baker, M. Temerin, G. D. Reeves, and R. D. Belian (1998), Simulation of dispersionless injections and drift echoes of energetic electrons associated with substorms, *Geophys. Res. Lett.*, *25*, 3763–3766.

Liang, J., W. W. Liu, E. Spanswick, and E. F. Donovan (2007), Azimuthal structures of substorm electron injection and their signatures in riometer observations, *J. Geophys. Res.*, *112*, A09209, doi:10.1029/2007JA012354.

Liang, J., E. F. Donovan, W. W. Liu, B. Jackel, M. Syrjasuo, S. B. Mende, H. U. Frey, V. Angelopoulos, and M. Connors (2008), Intensification of preexisting auroral arc at substorm expansion onset: Wave-like disruption during the first tens of seconds, *Geophys. Res. Lett.*, *35*, L17S19, doi:10.1029/2008GL033666.

Liu, W. W., J. Liang, E. Spanswick, and E. F. Donovan (2007), Remote-sensing magnetospheric dynamics with riometers: Observation and theory, *J. Geophys. Res.*, *112*, A05214, doi:10.1029/2006JA012115.

Luhmann, J. G., and L. M. Friesen (1979), A simple model of the magnetosphere, *J. Geophys. Res.*, *84*, 4405–4408.

Lui, A. T. Y. (1978), Estimates of current changes in geomagnetotail associated with a substorm, *Geophys. Res. Lett.*, *5*, 853–856.

Lui, A. T. Y., and J. R. Burrows (1978), Location of auroral arcs near substorm onsets, *J. Geophys. Res.*, *83*, 3342–3348.

Mauk, B. H., and C.-I. Meng (1987), Plasma injection during substorm, *Phys. Scr. T.*, *18*, 128–139.

McIlwain, C. E. (1974), Substorm injection boundaries, in *Magnetospheric Physics*, edited by B. M. McCormac, p. 143, Springer, New York.

Miyashita, Y., et al. (2009), A state-of-the-art picture of substorm-associated evolution of the near-Earth magnetotail obtained from superposed epoch analysis, *J. Geophys. Res.*, *114*, A01211, doi:10.1029/2008JA013225.

Nakamura, R., et al. (2009), Evolution of dipolarization in the near-Earth current sheet induced by earthward rapid flux transport, *Ann. Geophys.*, *27*, 1743–1754.

Newell, P. T., Y. I. Feldstein, Y. I. Galperin, and C.-I. Meng (1996), Morphology of nightside precipitation, *J. Geophys. Res.*, *101*, 10,737–10,748.

Panov, E. V., et al. (2010), Plasma sheet thickness during a bursty bulk flow reversal, *J. Geophys. Res.*, *115*, A05213, doi:10.1029/2009JA014743.

Reeves, G. D., T. A. Fritz, T. E. Clayton, and R. D. Belian (1990), Multi-satellite measurements of the substorm injection region, *Geophys. Res. Lett.*, *17*, 2015–2018.

Reeves, G. D., M. G. Henderson, P. S. McLachlan, R. D. Belian, R. Friedel, and A. Korth (1996), Radial propagation of substorm injections, *Eur. Space Agency Spec. Publ., ESA SP-339*, 579–584.

Samson, J. C., and P. Dobias (2005), Explosive instabilities and substorm intensifications in the Earth's magnetotail, in *Multiscale Coupling of Sun-Earth Processes*, edited by A. T. Y. Lui, Y. Kamide, and G. Consolini, pp. 135–251, Elsevier, Amsterdam.

Samson, J. C., and G. Rostoker (1983), Polarization characteristics of Pi2 pulsations and implications for their source mechanisms: Influence of the westward travelling surge, *Planet. Space Sci.*, *31*, 435–458.

Sarris, T. E., X. Li, N. Tsaggas, and N. Paschalidis (2002), Modeling energetic particle injections in dynamic pulse fields with varying propagation speeds, *J. Geophys. Res.*, *107*(A3), 1033, doi:10.1029/2001JA900166.

Sergeev, V. A., J. A. Sauvaud, H. Reme, A. Balogh, P. Daly, Q. Zong, V. Angelopoulos, M. Andre, and A. Vaivads (2003), Sharp boundary between the inner magnetosphere and active outer plasma sheet, *Geophys. Res. Lett.*, *30*(15), 1799, doi:10.1029/2003GL017095.

Shiokawa, K., W. Baumjohann, and G. Haerendel (1997), Braking of high-speed flows in the near-Earth tail, *Geophys. Res. Lett.*, *24*, 1179–1182.
Spanswick, E., E. Donovan, R. Friedel, and A. Korth (2007), Ground based identification of dispersionless electron injections, *Geophys. Res. Lett.*, *34*, L03101, doi:10.1029/2006GL028329.
Spanswick, E., et al. (2009), Global observations of substorm injection region evolution: 27 August 2001, *Ann. Geophys.*, *27*, 2019–2025.
Spanswick, E., G. D. Reeves, E. Donovan, and R. H. W. Friedel (2010), Injection region propagation outside of geosynchronous orbit, *J. Geophys. Res.*, *115*, A11214, doi:10.1029/2009JA015066.
Stern, D. P. (1970), Euler potentials, *Am. J. Phys.*, *35*, 494–501.
Summers, D., R. Tang, and R. M. Thorne (2009), Limit on stably trapped particle fluxes in planetary magnetospheres, *J. Geophys. Res.*, *114*, A10210, doi:10.1029/2009JA014428.
Toth, G., et al. (2005), Space Weather Modeling Framework: A new tool for the space science community, *J. Geophys. Res.*, *110*, A12226, doi:10.1029/2005JA011126.
Tsyganenko, N. A., and D. P. Stern (1996), Modeling the global magnetic field of the large-scale Birkeland current systems, *J. Geophys. Res.*, *101*, 27,187–27,198.
Wanliss, J. A., J. A. Samson, and E. Friedrich (2000), On the use of photometer data to map dynamics of the magnetotail current sheet during substorm growth phase, *J. Geophys. Res.*, *105*, 27,673–27,684.
Zaharia, S., J. Birn, R. H. W. Friedel, G. D. Reeves, M. F. Thomsen, and C. Z. Cheng (2004), Substorm injection modeling with nondipolar, time-dependent background field, *J. Geophys. Res.*, *109*, A10211, doi:10.1029/2004JA010464.
Zhu, P., J. Raeder, K. Germaschewski, and C. C. Hegna (2009), Initiation of ballooning instability in the near-Earth plasma sheet prior to the 23 March 2007 THEMIS substorm expansion onset, *Ann. Geophys.*, *27*, 1129–1138.

E. Donovan and E. Spanswick, Department of Physics and Astronomy, University of Calgary, 2500 University Dr., Calgary, AB T2N 1N4, Canada. (eric@phys.ucalgary.ca; emma@phys.ucalgary.ca)
K. Kabin, Department of Physics, Royal Military College of Canada, PO Box 17000 STN Forces, Kingston, ON K7K 7B4, Canada. (konstantin.kabin@rmc.ca)
R. Rankin and J. C. Samson, Department of Physics, University of Alberta, 11322-89 Ave., Edmonton, AB T6G 2G7, Canada. (rrankin@ualberta.ca; samson@phys.ualberta.ca)